Supplementary Information

$Ba_{1-x}Sr_xFeO_{3-\delta}$ as an Improved Oxygen Storage Material for Chemical Looping Air Separation: A Computational and Experimental Study

Shree Ram Acharya*[a,b]; Eric J. Popczun[a,b]; Hari P. Paudel[a,b]; Sittichai Natesakhawat[a,b]; Jonathan W. Lekse[a]; Yuhua Duan[a]

[a]National Energy Technology Laboratory, United States Department of Energy, 626 Cochran Mill Road, Pittsburgh, PA 15236, USA.
[b]NETL Support Contractor, 626 Cochran Mill Road, Pittsburgh, PA 15236, USA

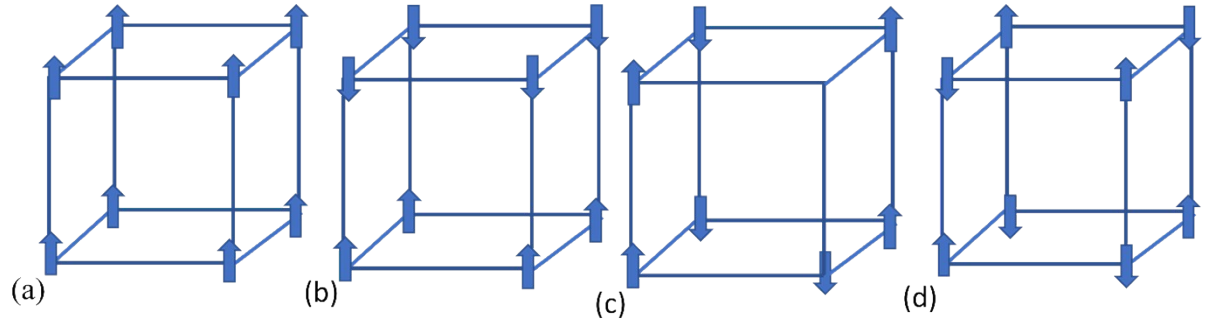

Fig. S1. Schematic representation of the four different magnetic states tested computationally in this study: (a) Ferromagnetic (FM), (b) *A*-type anti-ferromagnetic (*A*-AFM), (c) *C*-AFM, and (d) *G*-AFM.

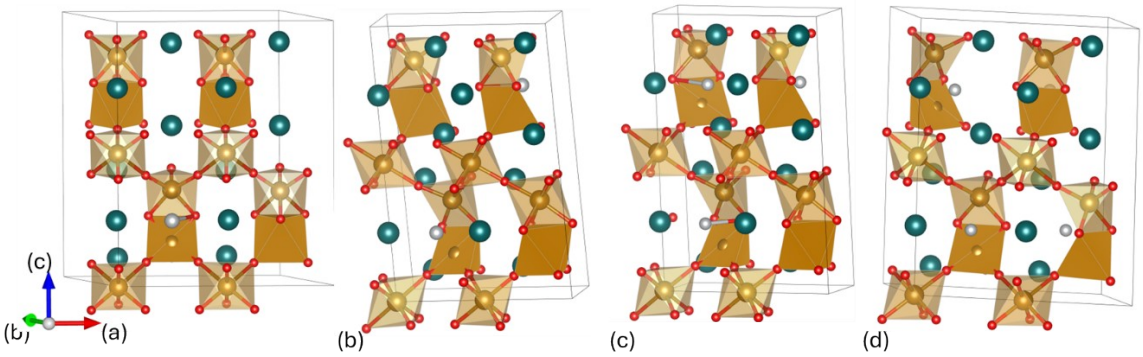

Fig. S2. Atomistic models of (a) $BaFeO_{2.917}$, (b) $BaFeO_{2.834}$, (c) $BaFeO_{2.75}$, and (d) $BaFeO_{2.667}$ OSMs. The green, gold, and red, spheres represent Ba, Fe, and O lattice sites, respectively. The oxygen vacancy sites are shown with sphere (gray colored) for visual convenience.

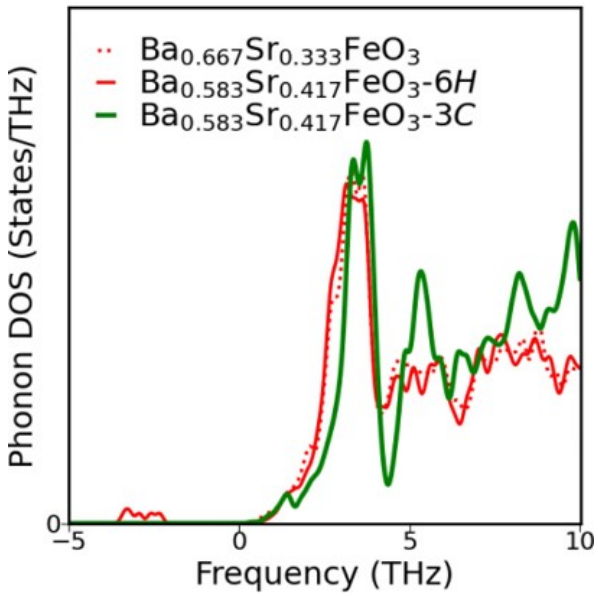

Fig. S3. The phonon density of states of $Ba_{1-x}Sr_xFeO_{3-\delta}$ (x = 0.333, 0.417) OSMs in hexagonal and cubic phases. The phonon density of states of $Ba_{0.583}Sr_{0.417}FeO_3$ depicts that the OSM in cubic phase are stable but the hexagonal phase is unstable due to presence of vibrational mode with imaginary frequency.

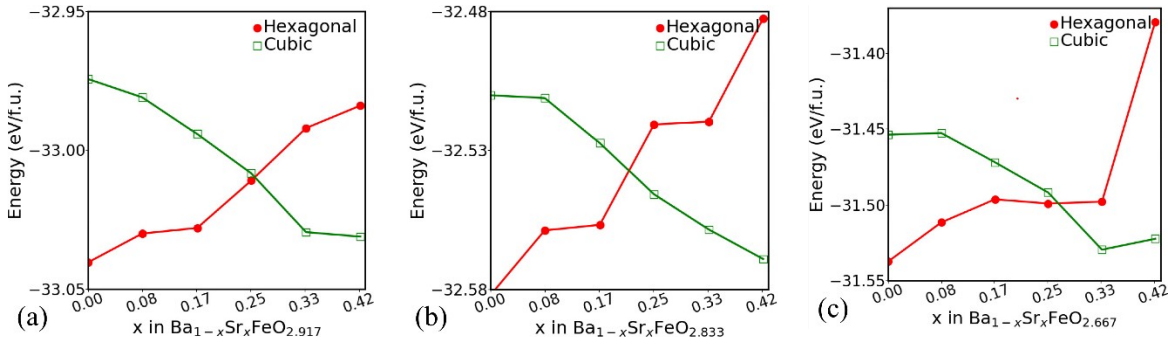

Fig. S4. Variation of energy per formula unit of the (a) $Ba_{1-x}Sr_xFeO_{2.917}$ (b) $Ba_{1-x}Sr_xFeO_{2.833}$ and (c) $Ba_{1-x}Sr_xFeO_{2.667}$ formed on hexagonal and cubic based phases with concentration of substituted Sr cations at x = 0.083, 0.167, 0.25, 0.333, and 0.417.

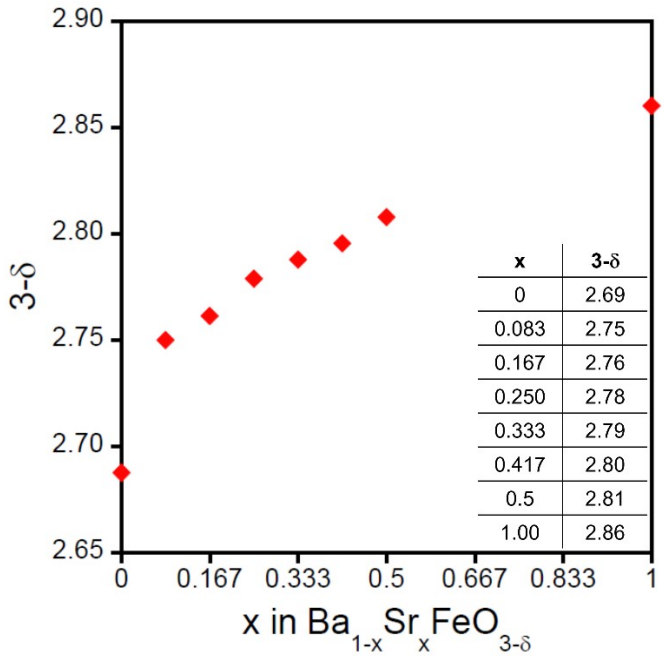

x	3-δ
0	2.69
0.083	2.75
0.167	2.76
0.250	2.78
0.333	2.79
0.417	2.80
0.5	2.81
1.00	2.86

Fig. S5. Oxygen stoichiometry of as-synthesized systems determined by thermogravimetric analysis. We observe a consistent increase of 3-δ as the Sr^{2+} content is increased. The hexagonal phase in $BaFeO_{2.69}$ is consistent with Parras et al.[1].

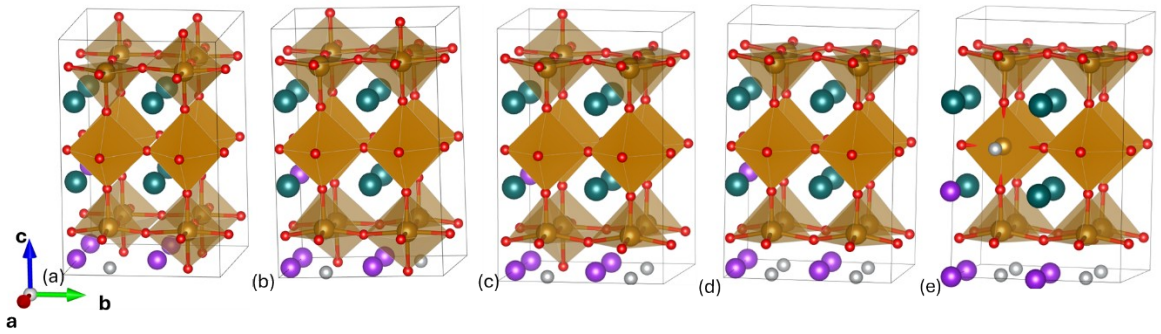

Fig. S6. Atomistic models of $Ba_{0.583}Sr_{0.417}FeO_{3-\delta}$ OSMs for (a) δ = 0.083, (b) δ = 0.167, (c) δ = 0.25, (d) δ = 0.333, and (e) δ = 0.5. The green, gold, red, and gray spheres represent Ba, Fe, O, and oxygen vacancy sites, respectively. At Sr substitution concentration (x) of 0.417, the cubic $Ba_{1-x}Sr_xFeO_{3-\delta}$ OSMs are energetically preferred. As shown in (a-e), structures with oxygen vacancies at the apical sites are energetically preferred. Note the co-planar arrangement of the substituted Sr^{2+} cations and the oxygen vacancies in these models.

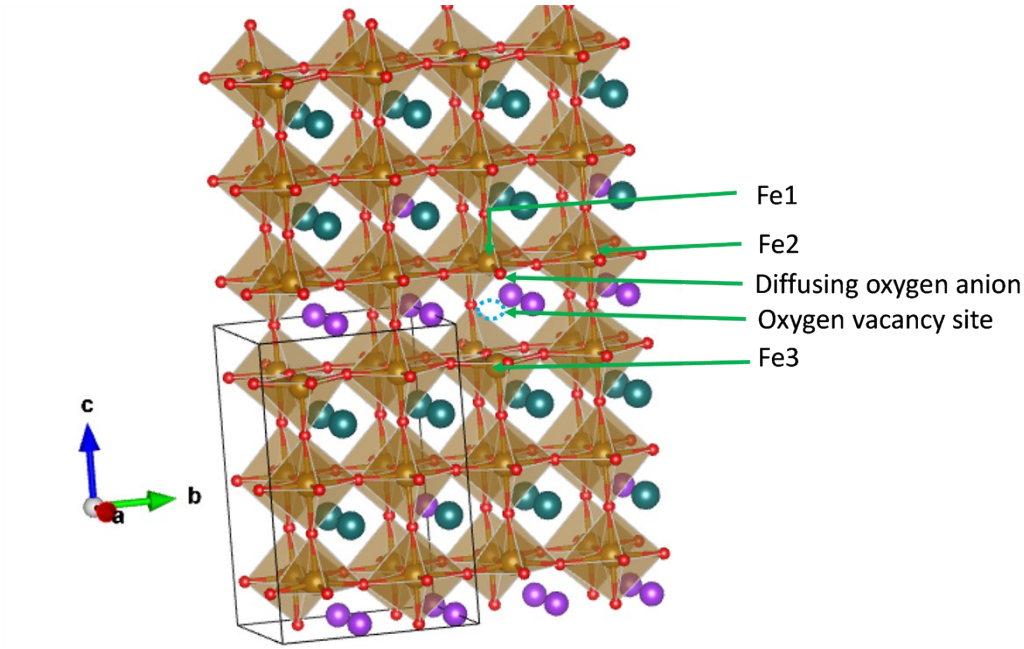

Fig. S7. The supercell model of the $Ba_{0.583}Sr_{0.417}FeO_{2.958}$ to show the diffusing oxygen anion on equatorial plane, it's targeted oxygen vacancy site on apical plane, and the nearby Fe atoms whose distance to diffusing oxygen anion are reported in table S3. The Fe1 and Fe2 are Fes nearby the diffusing oxygen on the same plane in initial configuration while Fe3 is close to the oxygen vacancy site.

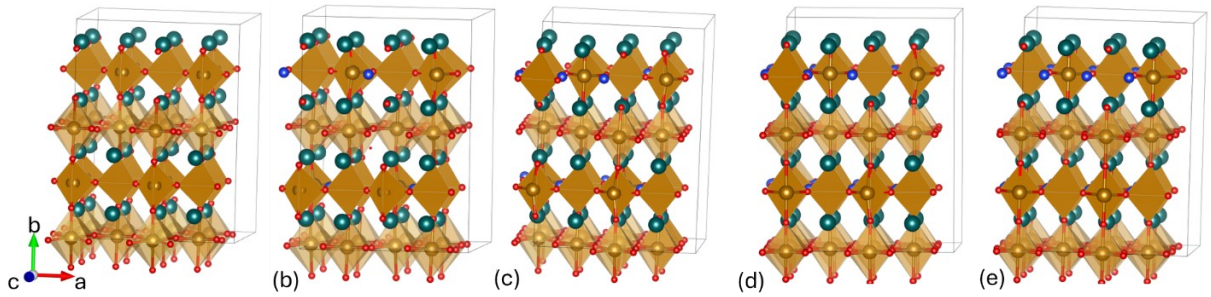

Fig. S8. Atomistic models of $BaFeO_{2.5+\delta}$ OSMs for (a) δ = 0, (b) δ = 0.125, (c) δ = 0.25, (d) δ = 0.375, and (e) δ = 0.5. The green, gold, red, and small sized blue spheres represent Ba, Fe, O, and absorbed oxygen that oxidize brownmillerite structure, respectively.

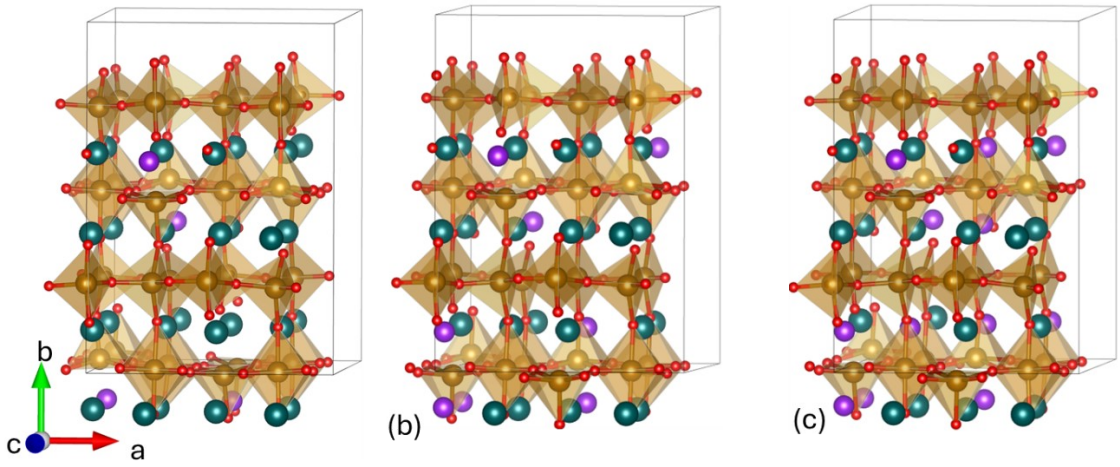

Fig. S9. Atomistic models of $Ba_{1-x}Sr_xFeO_{2.5}$ OSMs with (a) x = 0.125, (b) x = 0.25, and (c) x = 0.375. The green, gold, red, and purple spheres represent Ba, Fe, O, and Sr atoms, respectively.

Table S1. The difference of total energy per formula unit (ΔE) of three representative compounds namely $BaFeO_3$ of pristine system, $Ba_{0.583}Sr_{0.417}FeO_3$ of Sr substituted system, and $Ba_{0.583}Sr_{0.417}FeO_{2.917}$ of Sr substituted with oxygen vacancy system in *A*- type antiferromagnetic (*A*-AFM), *C*-AFM, *G*-AFM, and non-magnetic configurations relative to that of ferromagnetic (FM) configuration. The positive values imply the energetic preference of FM configuration.

Compound	ΔE(*A*-AFM)	ΔE(*C*-AFM)	ΔE(*G*-AFM)	ΔE(Non-Magnetic)
$BaFeO_3$	80	143	247	2813
$Ba_{0.583}Sr_{0.417}FeO_3$	78	173	271	2755
$Ba_{0.583}Sr_{0.417}FeO_{2.917}$	35	106	165	2733

Table S2. The lattice parameters of the stoichiometric $Ba_{1-x}Sr_xFeO_{3-\delta}$ OSMs on hexagonal and cubic phases. The measured values reported in Clemens et al.[2] are given in parentheses.

$Ba_{1-x}Sr_xFeO_{3-\delta}$	δ	Hexagonal				Cubic			
		a (Å)	*b* (Å)	*c* (Å)	Vol. (Å^3)	*a* (Å)	*b* (Å)	*c* (Å)	Vol. (Å^3)
x = 0.083	0	5.639 (5.654)	5.641	13.795 (13.906)	63.337	3.947	3.947	3.954	61.592
	0.083	5.646	5.654	13.865	63.856	3.955	3.955	3.945	62.026
	0.167	5.652	5.678	13.933	63.489	3.961	3.961	3.978	62.397
	0.25	5.669	5.685	14.015	63.106	3.955	3.955	4.032	63.075
	0.333	5.715	5.718	14.021	65.801	3.962	4.007	4.058	64.431
x = 0.167	0	5.623 (5.634)	5.625	13.779 (13.882)	62.897	3.937	3.938	3.945	61.161
	0.083	5.633	5.637	13.837	63.397	3.949	3.947	3.948	61.541
	0.167	5.648	5.642	13.905	63.981	3.966	3.937	3.967	61.945
	0.25	5.657	5.660	13.896	64.211	3.985	3.954	3.958	62.358

	0.333	5.656	5.705	13.928	65.028	4.012	3.937	3.979	62.852
x = 0.25	0	5.609	5.607	13.760	62.464	3.929	3.929	3.933	60.722
	0.083	5.620	5.626	13.830	63.068	3.939	3.939	3.932	61.028
	0.167	5.639	5.631	13.889	63.605	3.943	3.943	3.951	61.422
	0.25	5.647	5.649	13.947	64.292	3.939	3.939	3.976	61.675
	0.333	5.654	5.684	13.929	64.727	3.982	3.945	3.952	62.085
x = 0.333	0	5.592	5.592	13.736	61.996	3.919	3.919	3.923	60.262
	0.083	5.606	5.617	13.799	62.720	3.931	3.931	3.917	60.529
	0.167	5.630	5.638	13.850	63.354	3.956	3.912	3.924	60.707
	0.25	5.653	5.641	13.885	63.826	3.928	3.928	3.956	61.041
	0.333	5.689	5.676	13.903	64.517	3.932	3.932	3.959	61.209
x = 0.417	0	5.578	5.578	13.712	61.576	3.909	3.909	3.913	59.804
	0.083	5.589	5.593	13.782	62.165	3.921	3.921	3.909	60.093
	0.167	5.604	5.619	13.823	62.857	3.924	3.924	3.927	60.489
	0.25	5.632	5.638	13.778	63.251	3.919	3.919	3.949	60.664
	0.333	5.639	5.658	13.808	63.697	3.922	3.922	3.956	60.857

Table S3. The variation of the distance of diffusing oxygen to nearby Fe in $Ba_{0.583}Sr_{0.417}FeO_{2.958}$ and $Sr_{0.75}Ca_{0.25}FeO_{2.958}$ at different reaction coordinates in the diffusion pathway from equatorial site to vacancy on apical site. The Fe1, Fe2 and Fe3 cations are labelled Fig. S7.

Rxn. Coor.	$Ba_{0.583}Sr_{0.417}FeO_{2.958}$			$Sr_{0.75}Ca_{0.25}FeO_{2.958}$		
	d(Fe1-O)(Å)	*d*(Fe2-O)(Å)	*d*(Fe3-O)(Å)	*d*(Fe1-O)(Å)	*d*(Fe2-O)(Å)	*d*(Fe3-O)(Å)
0	1.88	2.094	4.201	1.853	2.004	4.039
1	1.805	2.385	3.811	1.843	2.068	3.792
2	1.753	2.799	3.334	1.801	2.421	3.311
3	1.744	3.255	2.857	1.777	2.94	2.754
4	1.765	3.608	2.49	1.801	3.286	2.367
5	1.816	3.933	2.151	1.842	3.595	2.059
6	1.850	4.188	1.995	1.856	3.809	1.949

Table S4. The DFT computed energy (per f.u.), lattice parameters, and volume of $Ba_{1-x}Sr_xFeO_{2.5+\delta}$ OSMs.

Compound	δ	*E* ($Ba_{1-x}Sr_xFeO_{2.5+\delta}$) (eV/f.u.)	*a* (Å)	*b* (Å)	*c* (Å)	Vol. (Å^3)
$BaFeO_{2.5+\delta}$	0.0	-30.301	5.804	15.560	5.891	531.99
	0.125	-31.167	5.733	15.741	5.768	520.42
	0.25	-31.958	5.696	15.846	5.671	511.86

	0.375	-32.682	5.653	15.790	5.646	503.96
	0.5	-33.372	5.668	15.625	5.668	502.04
$Ba_{0.75}Sr_{0.25}FeO_{2.5+\delta}$	0.0	-30.358	5.723	15.668	5.828	522.72
	0.125	-31.200	5.616	16.087	5.670	512.32
	0.25	-31.983	5.566	16.421	5.596	511.48
	0.375	-32.711	5.585	15.745	5.586	491.28
	0.5	-33.441	5.555	15.716	5.555	484.99
$Ba_{0.5}Sr_{0.5}FeO_{2.5+\delta}$	0.0	-30.408	5.573	16.417	5.706	522.06
	0.125	-31.211	5.561	16.081	5.616	502.24
	0.25	-31.981	5.515	16.334	5.547	499.69
	0.375	-32.726	5.545	15.633	5.545	480.62
	0.5	-33.475	5.516	15.582	5.516	474.15

Table S5. The oxygen storage capacity (OSC), reduction rate (Red. Rate), and oxidation rate (Ox. Rate) of $Ba_{1-x}Sr_xFeO_3$ at 325 °C and 350 °C using results of cyclic TGA measurements shown in Fig. 10. Reduction rate and oxidation rate were determined by the difference in mass after the first minute of reduction or oxidation, respectively. The values listed for $Sr_{0.7}Ca_{0.3}FeO_3$ are included for comparison.

Oxygen Storage Material	OSC (325°C, wt%)	Red. Rate (325°C, wt%/min)	Ox. Rate (325°C, wt%/min)	OSC (350°C, wt%)	Red. Rate (350°C, wt%/min)	Ox. Rate (350°C, wt%/min)
$BaFeO_3$	0.670%	0.021%	0.051%	0.935%	0.070%	0.104%
$Ba_{0.92}Sr_{0.08}FeO_3$	0.453%	0.006%	0.011%	0.945%	0.040%	0.051%
$Ba_{0.83}Sr_{0.17}FeO_3$	0.874%	0.020%	0.083%	1.213%	0.070%	0.243%
$Ba_{0.75}Sr_{0.25}FeO_3$	0.792%	0.012%	0.107%	1.098%	0.092%	0.353%
$Ba_{0.67}Sr_{0.33}FeO_3$	0.614%	0.020%	0.109%	0.906%	0.072%	0.335%
$Ba_{0.58}Sr_{0.42}FeO_3$	0.568%	0.020%	0.114%	0.840%	0.053%	0.338%
$Ba_{0.5}Sr_{0.5}FeO_3$	0.559%	0.028%	0.149%	0.803%	0.080%	0.412%
$SrFeO_3$	0.932%	0.032%	0.129%	0.902%	0.145%	0.536%
$Sr_{0.7}Ca_{0.3}FeO_3$	0.593%	0.016%	0.059%	1.323%	0.041%	0.125%

References:

1. M. Parras, M. Vallet-Regi, J.M. Gonzalez-Calbet, and J.C. Grenier, *Oxygen Vacancy Distribution in 6H $BaFeO_{3-\gamma}$ ($0.20 \leq \gamma \leq 0.35$),* J. Solid. State. Chem. 1989, **83**, 121-131.
2. O. Clemens, R. Haberkorn, P. R. Slater, and H. P. Beck, *Synthesis and Characterisation of the $Sr_xBa_{1-x}FeO_{3-y}$-System and the Fluorinated Phases $Sr_xBa_{1-x}FeO_2F$*, Solid State Sci., 2010, **12**, 1455.